# Chapter 11

# Comparisons of Different Methods

## 11.1 Objective

In double-frequency measurements, not only the ionospheric effects are involved, but also other effects which constitutes error sources in the double-frequency TEC measurements. Since separating between the effects of the ionosphere and the other effects is not trivial, in this thesis an investigation is done. The approach that is chosen is to compare different techniques for TEC measurement. The methods considered include measurements with different GNSS receivers by different manufacturers, measurements with Incoherent Scatter Radar (ISR), estimates performed with a network of different receivers. This last technique is applied for instance to compute the JPL global TEC maps, which exist for different times of the year and of the day. These comparisons have been described in (IV).

In order to enable comparisons with a ISR, the GNSS measurements analyzed here were done in Arecibo, Puerto Rico, at the Arecibo Observatory.
Aknownledgments go to Dr Sulzer and Dr Morton, which provided the data from the ISR, and to Dr Pelgrum and Dr van Graas, that made the GNSS data collections. A special thank to Dr van Graas that offered me the possibility to take part in this exciting work.

## 11.2 Noise and multipah mitigation through Modified CNMP algorithm

The modified CNMP algorithm [93], which was designed for dual-frequency differential GPS precision approach and landing, is here applied for TEC measurement scope.
The operating principle of the CNMP algorithm is based on the fact that the ionosphere-corrected Code Minus Carrier (CMC) is the sum of pseudorange noise, multipath, phase noise and a bias, which represents a combination of the residual carrier phase ambiguity and the clock offset. The algorithm aims to exchange the pseudorange noise and multipath for the noise present on the measured accumulated Doppler plus a bias. This operation results to be advantageous, since the effects of noise and multipath are smaller on the measurements of accumulated Doppler than on the measured pseudoranges. Furthermore, the additive contribution of bias is reducible.
Note that in the following the pseudoranges are indicated as $PR$ and the acccumulated Doppler as $AD$.
The pseudorange measurement is affected by several error components. It is:

$$\begin{aligned} PR_{Li}(t) &= R(t) + I_{Li}(t) + T(t) + \\ &\quad +\varepsilon_P(t) + \tau_{PR,Li}(\theta(t),\psi(t)) + \\ &\quad + c\Delta t_{PR,Li}(t) + \eta_{PR,Li}(t) \end{aligned} \tag{11.1}$$

where $I_{Li}(t)$ is the ionosphere delay, $T(t)$is the troposphere delay, $\varepsilon_P(t)$ is the satellite orbit error projected onto the line-of-sight, $\tau_{PR,Li}(\theta(t),\psi(t))$ is the antenna group delay as a function of elevation and azimuth angles, $\Delta t_{PR,Li}(t)$ is the receiver clock offset for the pseudorange and $\eta_{PR,Li}(t)$ represents the noise and multipath errors.
The measured AD gives an estimate of the true range plus a bias. The bias component is due to an ambiguity given by the unknown number $N$ of integer wavelengths between the user and the satellite, as described in Chapter 1. The AD measurement is affected by other undesirable effects, and it can be expressed,

similarly to the PR measurement, as:

$$\begin{aligned} AD_{Li}(t) &= R(t) - I_{Li}(t) + \\ &+ \frac{\lambda_{Li}}{2\pi}\psi(t) + T(t) + \varepsilon_P(t) + \\ &+ \tau_{AD,Li}(\theta(t), \psi(t)) + \\ &+ N_{Li}(t)\lambda_{Li} + \\ &+ c\Delta t_{AD,Li}(t) + \eta_{AD,Li}(t) \end{aligned} \tag{11.2}$$

where $N_{Li}(t)\lambda_{Li}$ represents the bias due to the integer ambiguity.

The ionosphere corrected CMC on the *i-th* frequency is

$$CMC_{Li,corr}(t) = PR_{Li}(t) - AD_{Li}(t) - 2I_{Li}(t) \tag{11.3}$$

i.e.:

$$\begin{aligned} CMC_{Li,corr}(t) &\approx \eta_{PR,Li}(t) + \tau_{PR,Li}(\theta(t), \psi(t)) + \\ &- 4.09\eta_{AD,L1}(t) + 3.09\eta_{AD,L2}(t) + B \end{aligned} \tag{11.4}$$

where the bias $B$ includes the unsolved integer ambiguity.
An estimate $\hat{B}(t)$ of the bias $B$ can be computed as an average over time of $CMC_{Li,corr}(t)$. An averaging window of 1000 seconds is used, so that it is longer than the period of the multipath component with the slowest frequency, considered to be higher than 1/1000 Hz. In order to eliminate components with fading periods shorter than 1000 s, a low-pass filter is applied on $CMC_{Li,corr}(t)$.
The corrected pseudorange is then obtained by subtracting from the pseudorange measurement as in (11.1) the CMC measurement as in (11.4) and the bias estimate $\hat{B}(t)$:

$$\begin{aligned} PR_{Li,CNMP}(t) &= R(t) + I_{L1}(t) + \\ &+ T(t) + \varepsilon_P(t) + \\ &+ c\Delta t_{PR,Li}(t) + 4.09\eta_{AD,L1}(t) + \\ &- 3.09\eta_{AD,L2}(t) - B + \hat{B}(t) \end{aligned} \tag{11.5}$$

The goodness of the estimate $\hat{B}(t)$ depends on how much the mean of the noise and in particular the multipath contributions on the true bias $B$ differs from zero, over that time interval. The more biased the noise and the multipath are, the bigger the error on the bias estimate is.
An over-bound on the bias estimate can be determined, considering the worst

case of all the error contributions, i.e. PR noise, noise on the AD, antenna group delay and multipath.

Taking into account the bandwidth of the receiver loops, the bound on the noise can be initialized at 31.2 cm, a value which can be decreased, after five minutes of lock without interruptions, to 3.1 cm (see [93] for details). The bound for the antenna group delay can be considered, for ground receivers, 10 cm.

The multipath contribution at the initialization time has the largest bound, but it can be decreased over time.

The bound on the amplitude of the ground multipath can be found as:

$$MP_{PR} = \ 2h\sin(\theta)\frac{\gamma}{(1-\gamma)} \tag{11.6}$$

where $\theta$ is the elevation of the satellite and $h$ (in this case $h = 3$ m) is the height of the antenna above the ground surface in meters, while $\gamma < 1$ is the MP-to-direct strength ratio.

In this case it is $MP_{PR_{init}} = \ 2$ m. Hence the initial bound is $MP_{bo,init} = 2 + 0.312 + 0.10 \ = \ 2.41$ m, that can be reduced by evaluating more accurately $MP_{PR}$. After the filtering of $CMC_{Li,corr}(t)$, in order to bound the contribution of the multipath on the error, the maximum amplitude of the slower oscillations on $CMC$, which are likely to be due to the multipath, is evaluated as:

$$MP_{L1bo,new} = max\{CMC_{L1,c,f}\} - min\{CMC_{L1,c,f}\} \tag{11.7}$$

Iteratively, the MP bound is updated as the minimum between the current and the last computed bound:

$$MP_{L1bo,upd} = min\{MP_{L1bo,curr},\ MP_{L1bo,new}\}. \tag{11.8}$$

As long as continuous carrier tracking is maintained, the bias $B$ has an unknown but constant value during an observation, when a satellite is visible (up to about 6 hours). Therefore there is a specific time $t_B$ at which the bias estimate $\hat{B}(t_B)$ is the best one, corresponding to the bias estimate computed during the time interval of 1000 seconds with the most favorable bound, as shown in Figure 11.1. If the algorithm is run in real-time, then the bias estimate starts at the initial bound and become smaller as the actual multipath error is determined by the CNMP algorithm.

According to this method, the best epoch for the bias evaluation is the one when the effect of multipath is the smallest one, which usually corresponds to an epoch

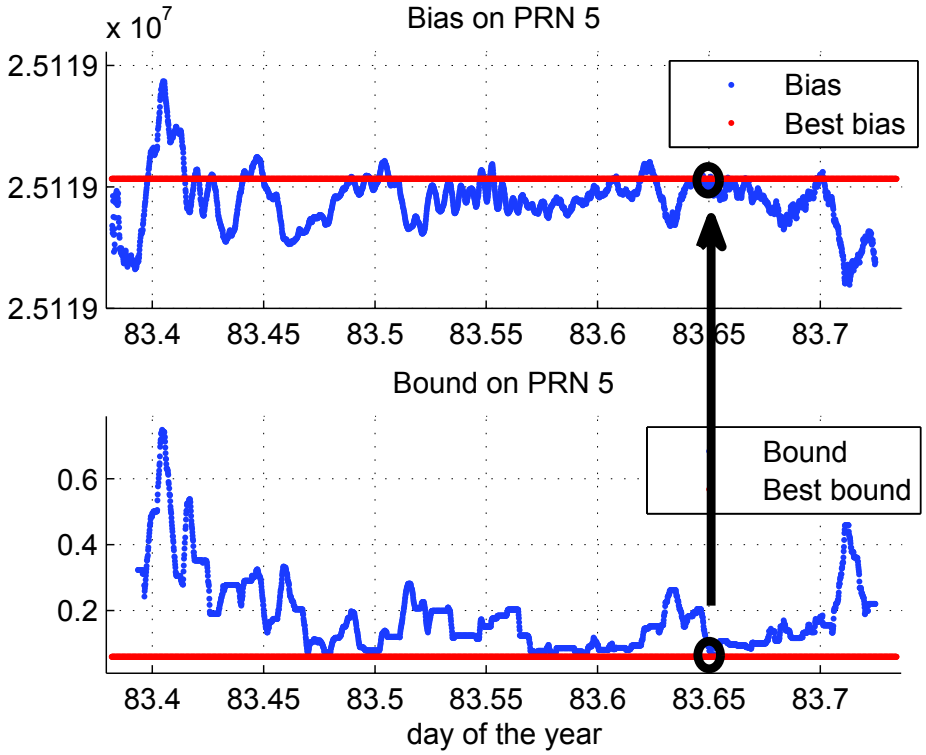


Figure 11.1: Bias (above) and Bound (below) on $\mathbf{PR_{L1}}$ filtered with the modified CNMP algorithm, in blue. The red plots are respectively the best bound and the corresponding best bias estimate. The black circles and the arrow highlight the minimum bound and the corresponding best bias estimated. The figure shows the result for PRN 5, Ashtech receiver.

when the satellite is at high elevation.

Figure 11.1 shows a comparison between the bound and the best bound found, for the PRN 5 on L1, for three different receivers. It can be noted how, as expected, the bound due to the multipath effect is very similar for the receivers in the same location, in the same time. This bias can thus be applied to the whole pseudorange measurement, so that the bound on the bias estimate results to be the same value for all the epochs, and the smallest bound found over the whole measurement.

With the filtered and bias-corrected L1 and L2 pseudoranges, the sTEC can be estimated, using the basic dual-frequency relationship expressed by (10.1), as:

$$sTEC_{CNMP}(t) = k\left(PR_{\min_{bo}L1}(t) - PR_{\min_{bo}L2}(t)\right) \tag{11.9}$$

In this way, using the filtered and bias-corrected pseudoranges measurements, a

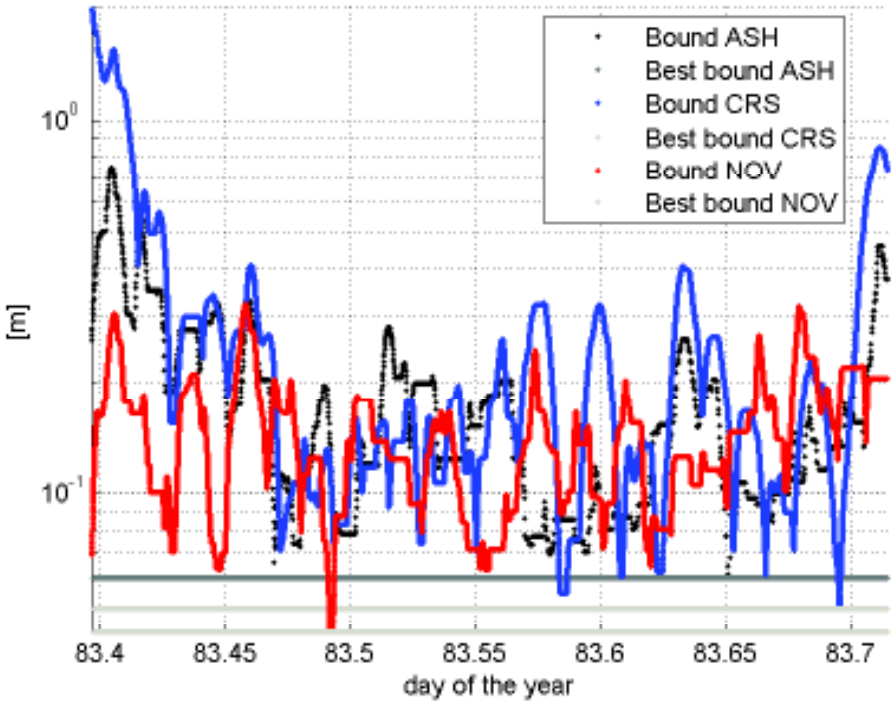


Figure 11.2: CNMP bound and minimum bound on L1, Log scale. Comparison between receivers.

filtered estimate of TEC can be obtained, as shown in Figure 11.3 and Figure 11.4, where the sTEC is computed for two satellites, with the Ashtech and the CRS receivers, respectively. In Figures 11.3 and 11.4 a comparison is shown between the standard dual-frequency measurements using raw PR measurements and the CNMP filtered TEC estimates.

Linearity can be applied to the bound on the bias estimate due to the multipath, from (11.9). The bound on the sTEC bias estimate, due to the multipath is:

$$MP_{\min_{bo}TEC} = k\,(MP_{\min_{bo}L1} + MP_{\min_{bo}L2}) \tag{11.10}$$

Figure 11.5 shows the CNMP bound on the TEC measurement with the Ashtech receiver, on PRN 5. The minimum bound is less than 1 TECU and this value represents a typical value found in this environment, for different GPS receivers.

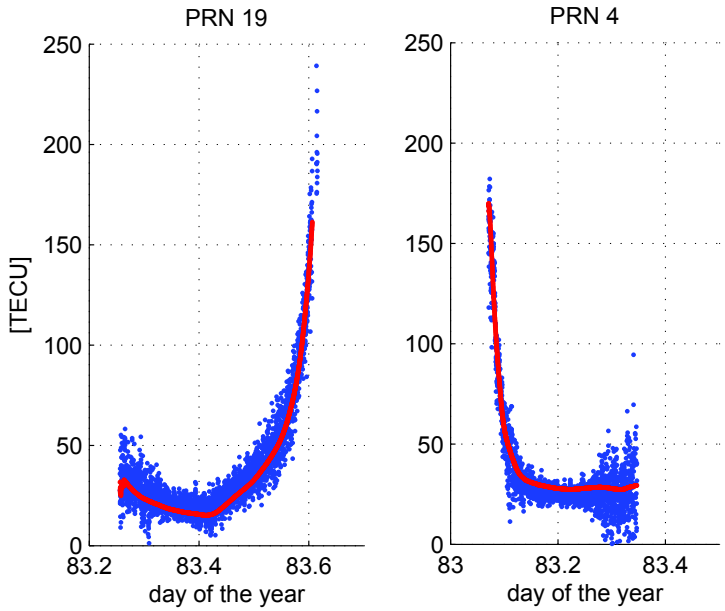


Figure 11.3: Comparison of raw (blue) and CNMP (red) Ashtech sTEC measurements. Satellite DCB corrected, for satellite 19 (left) and 4 (right).

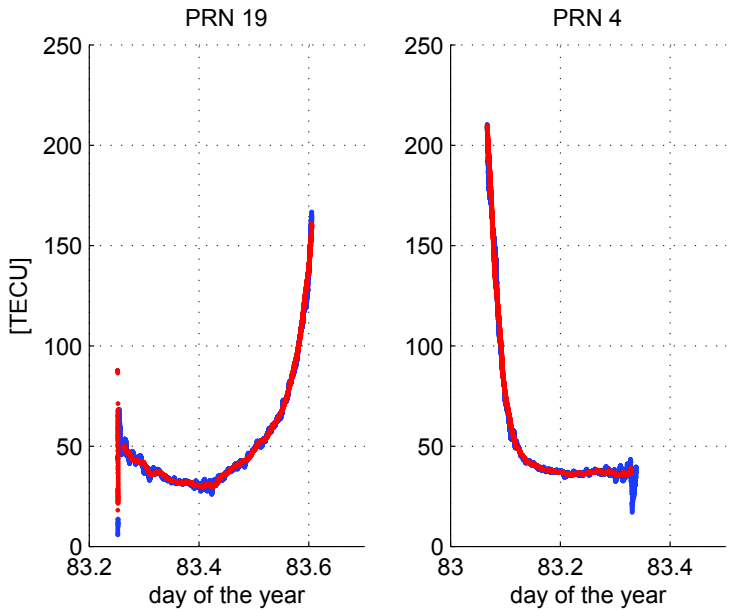


Figure 11.4: Comparison of raw (blue) and CNMP (red) CRS sTEC measurements. Satellite DCB corrected, for satellite 19 (left) and 4 (right).

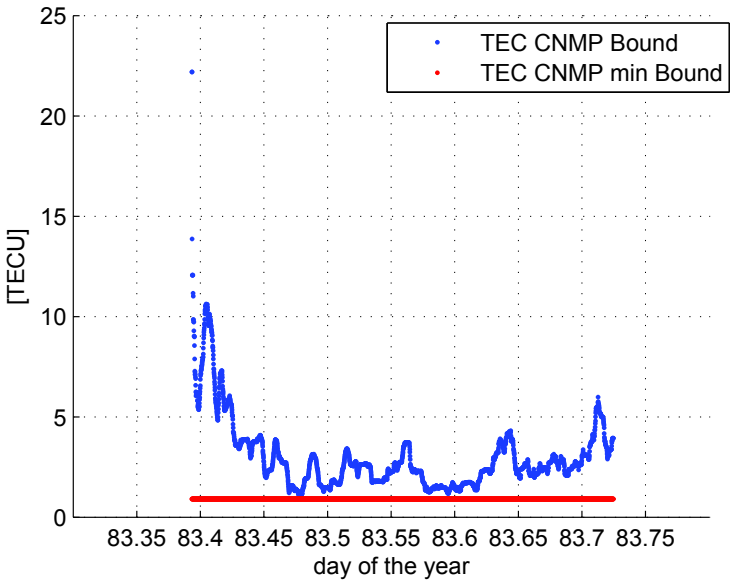


Figure 11.5: Bound (blue) on the TEC estimate and best bound (red). Ashtec receiver, PRN 5.

## 11.3 Satellite inter-code and inter-frequency biases mitigation

Satellite Differential Code Biases (DCB) are estimated and provided online by several organizations, as instance, by CODE [94]. The manual about the data in [94] is available in [95]. As explained in [96], the DCB provided by CODE is such that the corrected pseudorange difference in meters is given by the observed difference minus the bias correction:

$$\left(PR_{P_{L1}} - PR_{C/A_{L1}}\right)_c = \left(PR_{P_{L1}} - PR_{C/A_{L1}}\right)_o - cb \tag{11.11}$$

where $c$ is the speed of light.

CODE provides the DCBs $(P\,(Y))_{L1}-(C/A)_{L1}$ and the frequency bias $(P\,(Y))_{L1}-(P\,(Y))_{L2}$.

In this thesis, the second value is used to correct the TEC measurement performed by the receiver using the $P\,(Y)$ code both on L1 and L2 (Ashtech and CRS).

The combined inter-frequency and inter-code bias $(C/A)_{L1}-(P\,(Y))_{L2} = (P\,(Y))_{L1}-(P\,(Y))_{L2} - [(P\,(Y))_{L1} - (C/A)_{L1}\,]$ is computed to be used in the correction of the TEC measurement performed by receivers that use the $P\,(Y)$code on L2 and

$C/A$ on L1 (NovAtel and Septentrio).

Figure 11.6 shows the sTEC measurement with (blue) and without (red) the correction for the inter-code and inter-frequency biases, for CRS and NovAtel, respectively.

Due to the satellite bias, which is different for each satellite, the sTEC measurements differ significantly before the correction. After the correction of the satellite biases, the CRS performs better in terms of inter-frequency and inter-code bias, because the receiver inter-code and inter-frequency bias components are HW calibrated.

The NovAtel receiver shows a bigger bias between the satellites, and this could be due to the fact that CRS uses P(Y) code on L1 and on L2, while the NovAtel makes available P(Y) code on L2 but only C/A code on L1, therefore a further inter-code bias is present.

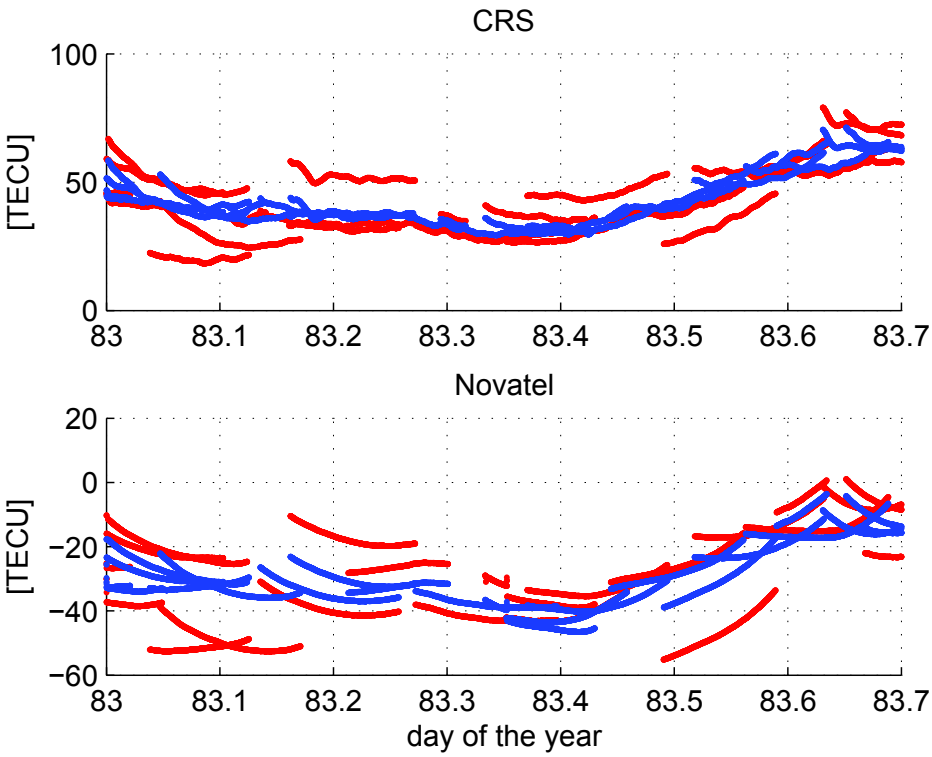


Figure 11.6: CRS (above) and NovAtel(below) sTEC measurements, CNMP filtered, without (red) and with satellite DCB mitigation. Notice that the CRS is corrected for the inter-frequency bias $\mathbf{PR_{P_{L1}}} - \mathbf{P}R_{\mathbf{P_{L2}}}$ while the NovAtel is corrected both for the inter-frequency and the inter-code bias $\mathbf{P}R_{\mathbf{C/A_{L1}}} - \mathbf{PR_{P_{L2}}}$.

## 11.4 Calibration methods overview

One of the largest error sources in the estimation of TEC using double-frequency GNSS measurements is the determination of the unknown receiver biases. In order to estimate these biases, several approaches are possible, some of which are described in the following paragraphs, as for example HW calibration or zero-TEC calibration.
Furthermore, in order to evaluate the uncertainty on the GNSS estimate, comparisons with other methods can be done, such as with the measurements obtained using the MAPGPS [88], the TEC maps provided by JPL, the ISR measurements, or occultation techniques.

### 11.4.1 Hardware calibration (CRS receiver)

The CRS receiver is equipped with a hardware calibration option for the receiver inter-frequency bias measurements.
In the receiver manual [97] it is said that the internal calibration included with the receiver is designed to measure receiver hardware delays to the mm level, with the aim of estimating TEC with bias estimates better than 0.1 TECU. As described in [97], in order to calibrate the internal HW delays, the receiver is connected to a signal simulator, so that the input signal is received without any errors due to the propagation path and ionospheric effects. The CRS HW calibration method and performance are detailed in [97].
If the antenna/pre-amp delays are constant and identical between L1 and L2, the CRS should provide the most accurate estimate, compared with others receivers that do not implement any calibration method.
Also other examples of calibration for TEC measurements exist in literature, as for example [98] where a simulator is used, or [99] where the receiver bias is estimated by comparison with a ionosonde. A completely different approach towards the ionosphere measurement and the receiver bias calibration is proposed as instance in [71].

### 11.4.2 Zero TEC method

A very simple and commonly used method to compensate for the receiver biases is known as zero-TEC.

The basic assumption is that the TEC is zero, or very close to zero, during the early morning hours, in particular around 6 a.m. local time, just before the sunrise, as a consequence of the reduced solar energy radiated in the ionosphere during the night time. According to this method, the vertical TEC computed during one day is calibrated by setting to zero the minimum TEC, which usually should be in between 5 and 7 a.m.
However, the assumption not to have any ionospheric activity when the ionosphere is quiet is not very accurate. This approach can improve the estimates of relative TEC measurements, between receivers and days, but it is not accurate in terms absolute TEC measurement, if a bias-free estimated is needed.
Other methods, such as some ionospheric models [91], [92], pone the hypothesis that the minimum TEC is a certain value $> 0$, which depends on the location on the earth and on the season.

### 11.4.3 MAPGPS

The MAPGPS (MIT Automated Processing of GPS), described in [88], is a software package developed at the MIT Haystack Observatory, able to produce reliable TEC data automatically, in post processing.
The approach of the MAPGPS to solving the problem of the unknown receiver bias determination makes use of three methods:

1. Minimum Scalloping, based on the assumption that the more accurate the estimated bias is, the more the sTEC computed from different satellites agree when converted into vTEC for the same location.

2. Least Squares, solving for the receiver bias under the hypothesis that it is constant during one day and for all the satellites, and that the bias of each satellite is perfectly known.

3. Zero-TEC, assuming that the minimum TEC value during the day (early in the morning) can be fairly approximated as 0 TECU.

The slant and vertical TEC data that the Arecibo Observatory makes available on the online database [12], for the Arecibo location, are computed using the MAPGPS method. Also, the graphics of TEC profiles available at [12] are based on the MAPGPS method.

### 11.4.4 JPL maps

The TEC global maps (an example is shown in Figure 11.7), produced by the NASA Jet Propulsion Laboratory (JPL), provides a tool to correct the ionospheric delay in any location on Earth, therefore is very important for single-frequency users. Furthermore, these maps constitute a ionospheric calibration for navigation systems, as well as a reference to compare other ionosphere monitoring methods.
The JPL TEC estimates are computed using data from a network of receivers, in particular, from about 100 real-time tracking sites constituing the NASA GDGPS (Global Differential GPS) plus data from other sites available every hour. Each receiver computes the sTEC along the LOS with the in-view satellites and these measurements from all the sites are then processed using a Kalman filter, to obtain a worldwide grid of TEC values.
The map grid is spaced at 2.5° in latitude and 5° in longitude. A global TEC map update is computed every 5 minutes, and a figure corresponding to the computed TEC map is available online [100] in real-time (updating rate: 5 minutes). Text files are also available online containing the TEC grids, but only 13 global TEC maps are available for each day (which means updating rate of 2 hours).

### 11.4.5 Arecibo Incoherent Scattering Radar

As introduced at the beginning of this chapter, in this thesis comparisons are shown between different GNSS TEC measurements taken in Arecibo, Puerto Rico, at the Arecibo Observatory, in order to compare the results with the measurements performed by the Incoherent Scatter Radar (ISR), shown in Figure 11.8.
The ISR in Arecibo belongs to the first generation of operational ISRs built in the early 1960s. These devices allow to monitor electron densities and drifts, temperatures and chemical composition of plasmas in the ionosphere. ISR measurements can be used also to find models for the inosphere behavior [101].
Unfortunately, the ISR measurement itself is also subject to calibration, which means that the absolute value of the TEC is not known accurately, due in particular to hardware calibration problems affecting the ISR.

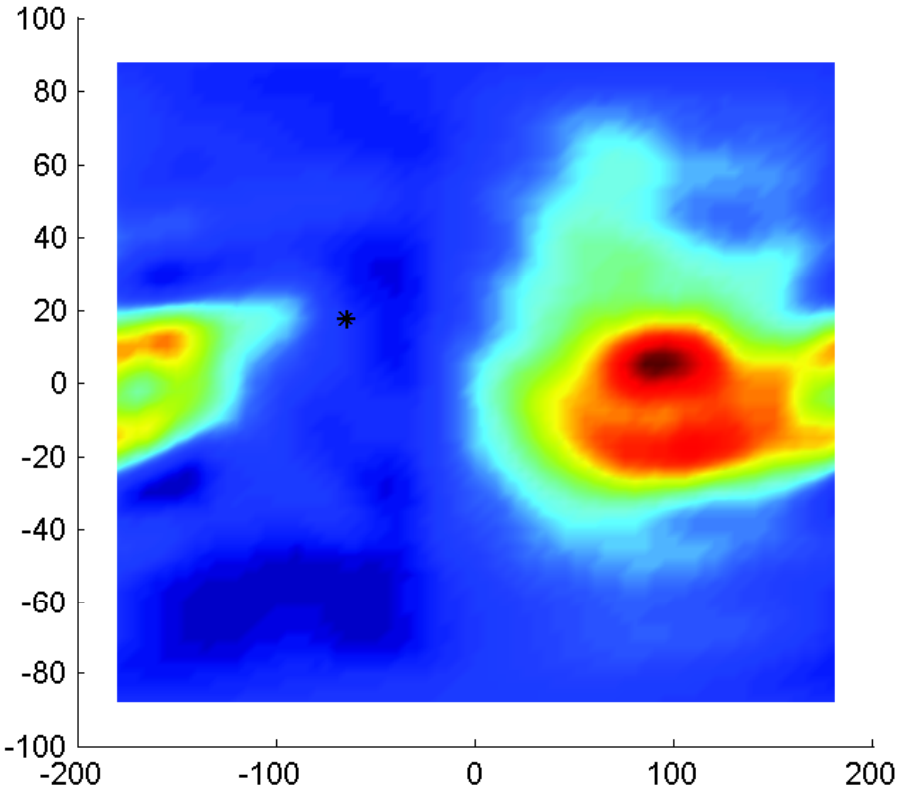


Figure 11.7: JPL map, day 84, slot time 5/13 (Arecibo local hour comprises between 4 a.m. and 6 a.m.). The white circle indicates the position of the Arecibo Observatory.

### Working principle

The ISR can measure vertical profiles of ionospheric electron content. This means that it can discriminate between various heights, differently from the GNSS measurements that can only provide an estimate of the total electron content along the whole line of sight user-satellite.

The physical mechanism at the basis of the ISR measurements is the Thomson scattering of electromagnetic waves, caused by the interaction of the electromagnetic waves with the free electrons in the ionosphere. The details of this theory are above the scope of this thesis, therefore it is not explained in detail here.

The possibility to apply the incoherent scattering principle of radio waves by free electrons to the radar space exploration was outlined at the end of the 1950s [102]. Radar pulses that incide on free electrons make them oscillating, and the signal

Figure 11.8: Incoherent Scatter Radar, Arecibo Observatory (Arecibo, Puerto Rico). Source online: National Astronomy and Ionosphere Center (Arecibo Observatory) [12].

is re-radiated from the oscillating electrons, that behave like Hertzian dipoles, at the frequency of the incident wave [103]. Each of the Thomson scattering electrons can be considered having statistically independent random motions, and it is to this kind of situation that the incoherent scatter concept is referred to. [104]. The power of the re-radiated waves depends on several factors, which are a direct function of the electron content distribution. This means that if a known amount of power is radiated, the measure of the received power due to scattered fields gives an estimate of the number of free electrons. Moreover, the frequency spectrum of the measured signal is affected by the two-way Doppler, which allows to discriminate the distance at which the scatter-effect that generated a wave with a certain power level took place. Thanks to this, vertical profiles are traceable. If the electrons could be considered as hard targets, the standard radar equation [105] could be applied, simply obtaining the total scattered power as a sum of the power scattered by each electron. Actually, the motion of ionospheric free electrons are not fully independent and the more the true configuration is far from satisfying the hypothesis, i.e., the more the electron

motions are correlated to each others, the worse the approximation given by the standard radar equation is.
Due to this approximation, what is called incoherent scatter radar is in reality a not-exactly-incoherent scatter radar. Realistic models exist, which fit better this kind of ionospheric radar measurements, involving particle correlated motions.
Several factors influence the correlation among the particles and the plasma dispersion, and therefore the quality of this approximation. These factors, apart the electron density, include also electron and ion temperature, electron/ion temperature ratio, mean ion mass and ion-neutral collision frequency.
All these factors, difficult to be modeled accurately, contribute to build up the uncertainty in the radar measurements.

### ISR measurements

Figure 11.9 and Figure 11.10 shows some ISR measurements taken in Arecibo in March $25^{th}$ 2011. The two figures show the same results, visualized in two different ways: Figure 11.9 show a different plot for different times of the day (the indicated time is the Arecibo local time, in the format hhmmss, i.e. hour, minute, second), indicating the measured value of Ne on the abscissa axis, for different elevations, on the ordinates axis. Figure 11.10 shows in 3D the measured Ne for different times and altitudes. Similarly, Figure 11.11 and Figure 11.12 report results obtained two days later, on March $27^{th}$ 2011. By integrating the electron content along all the altitudes, an estimate of vTEC can be found at each epoch, that can be compared with the GNSS measurement.

### Radar measurement error sources

The estimate error amount is highly related to the power spectral resolution. It is important to consider a model for the temperature of the ionosphere, which is connected also to the expected electron number, as for example the one proposed in [106], [104]. The measurement performance depends on several parameters. In particular the received SNR depends on several factors, including ISR operating frequency, transmitted peak power, transmitter duty cycle, receiver noise temperature and receiving antenna gain. The SNR is related to a given plasma density at a given range, therefore the time resolution of the ISR highly depend on the SNR. Moreover the receiver bandwidth and the collecting area influence

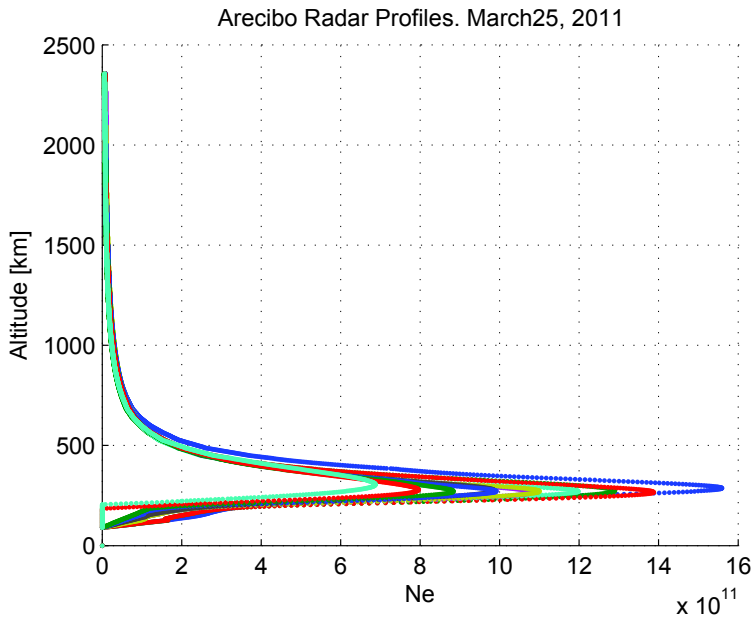


Figure 11.9: ISR vertical Profiles, Arecibo, March $25^{th}$ 2011, at different times.

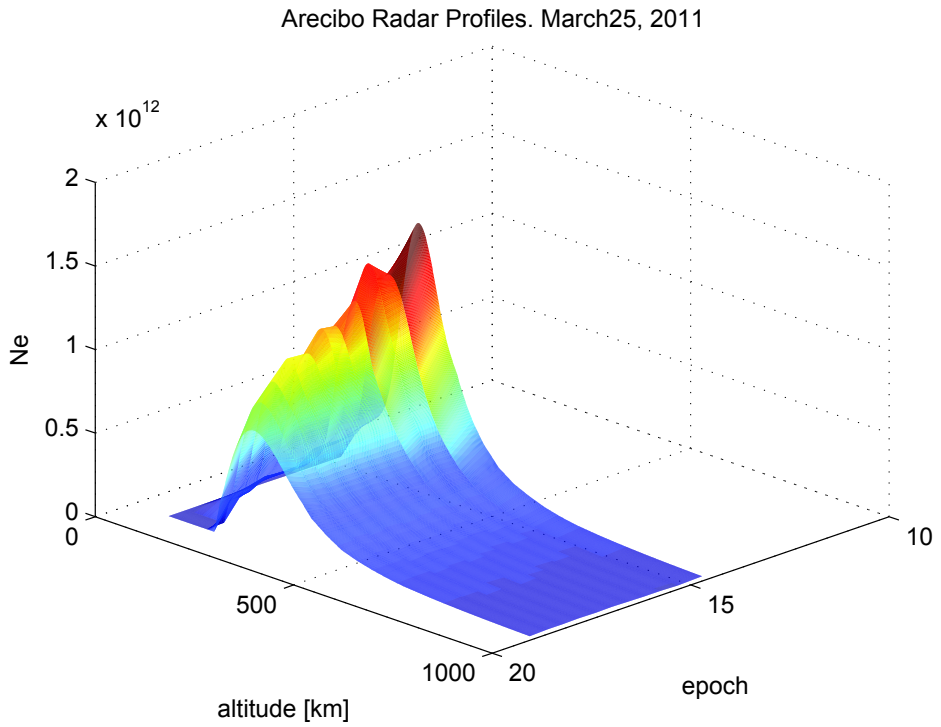


Figure 11.10: ISR TEC measurements, Arecibo, March $25^{th}$ 2011, at different times and different altitudes.

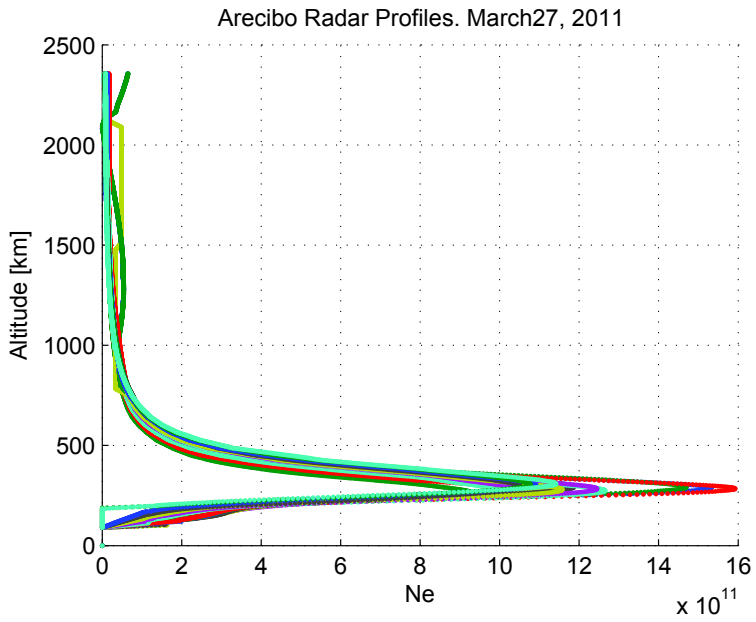


Figure 11.11: ISR vertical Profiles, Arecibo, March $27^{th}$ 2011.

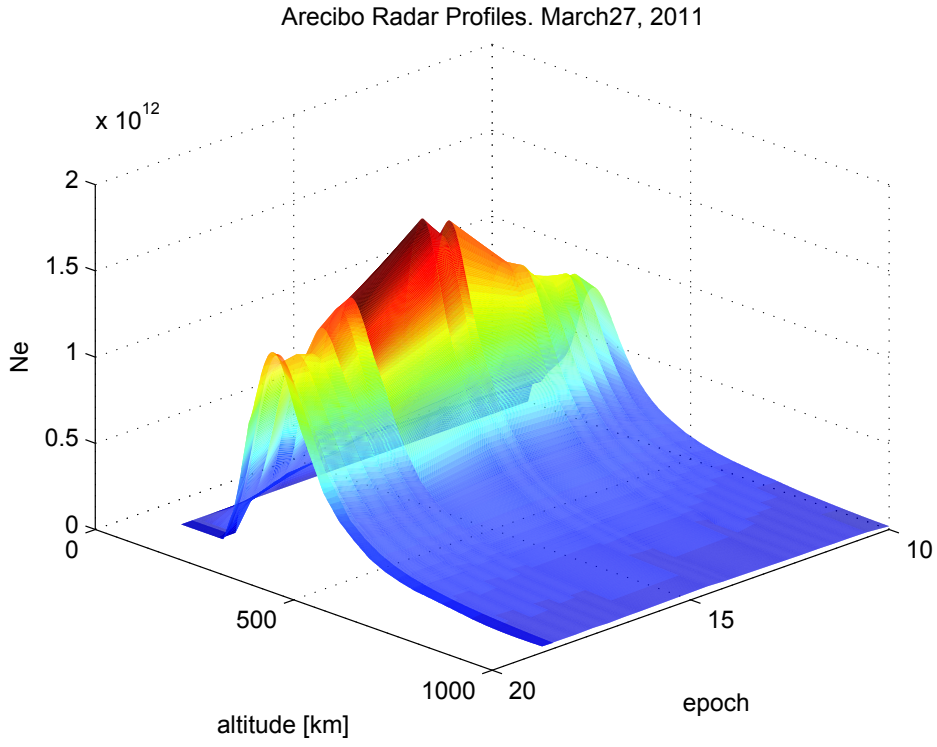


Figure 11.12: ISR TEC measurements, Arecibo, March $25^{th}$ 2011, at different times and different altitudes.

the performance. The transmitted pulse length (minimum and maximum) has an impact in terms of spatial resolution (altitude/range resolution).
However, the most critical parameter in terms of contribution to the TEC measurement bias is constituted by the ISR hardware biases. Concerning the ISR in Arecibo, there are not defined bounds on the measurement biases, in fact the main goal of the radar is to provide a monitoring of the ionosphere, without a specific requirement on the bias determination accuracy.
This means that the focus is mainly on the relative measurements, which allow to find the differences in the ionospheric behavior at different epochs and different heights, while not so much importance is given to the absolute measurement.
In [107] some error sources in the ISR are analyzed, but the problem of the residual hardware bias is not investigated.
Due to this, not many details about the HW calibration are available. In Section 11.5 it is shown that the measurements provided by the Arecibo Observatory look to be calibrated using a zero-TEC method, however, more analysis need to be done.
As a result, the comparisons that are shown in this thesis do not have the only aim to check the accuracy of the GNSS receiver estimate, but they could provide also a tool to investigate the measurement bias of other devices that measure the ionospheric TEC, such as the ISR.

### 11.4.6 Radio occultation

Radio occultation techniques can be used to evaluate the ionospheric TEC [108]. Different measurements can be combined in order to obtain vertical TEC profile. The advantages of the radio occultation techniques is that lots of error sources do not occur, first of all the multipath. Moreover, this method provides a different measurement, giving the estimate along a very different direction with respect to the measurements that a user on the earth can do, since for radio occultation techniques the line-of-sight is between two satellites, as shown in Figure 11.13. COSMIC (Constellation Observing System for Meteorology Ionosphere and Climate) is the result of a joint U.S.-Taiwanese project and provides the opportunity to combine GPS satellites with LEO satellites, to obtained measurements to be used in ionospheric research and also in meteorology, climatology and space weather.

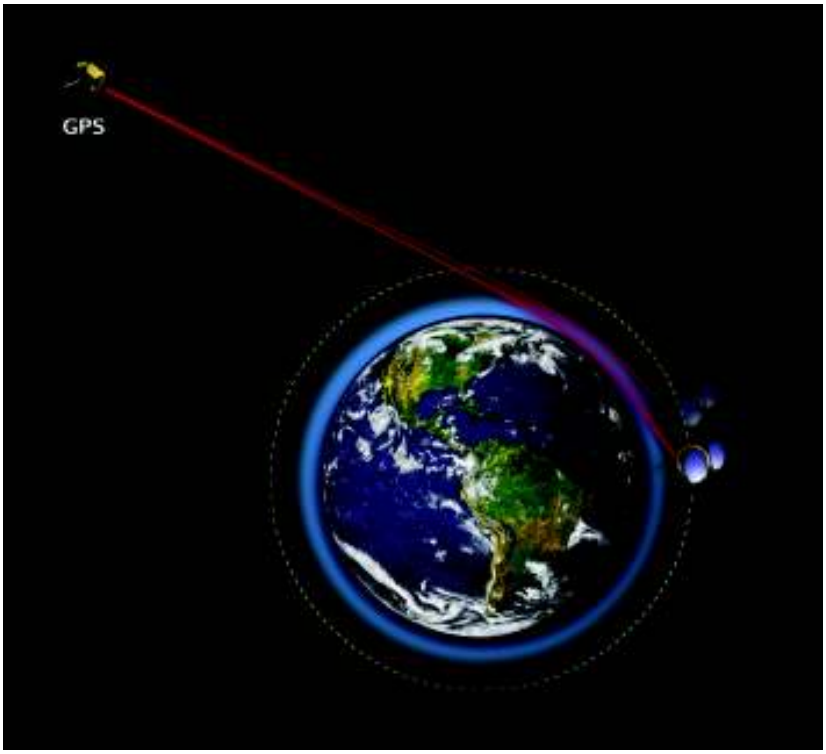


Figure 11.13: Radio Occultation for ionosphere monitoring. Source online: International Radio Occultation Working Group [13]

In this thesis the measurements from radio occultation techniques are not analyzed, but these techniques may be taken into account for future developments of the analysis.

## 11.5 Methods comparison

Figure 11.14 shows a comparison between the sTEC measurements from three receivers, compared with the data from MAPGPS. From Figure 11.14 it can be seen that a residual bias is present on the absolute sTEC estimates, due to the receivers.

Figure 11.15 shows the measurements calibrated with a zero-TEC technique. However, misalignments are still present, in particular because the minimum TEC value is not measured at the same time by all receivers. While the NovAtel measurement agrees with the MAPGPS method in detecting the minimum sTEC around 6 a.m. (local time), the CRS receiver finds the minimum TEC around 4.16 a.m. and the Ashtech around 5.36 a.m.

The time of the minimum according to the MAPGPS is here considered to be the minimum time of reference. The sTEC measured by each receiver is then calibrated by subtracting the corresponding value computed at that time. In this way, the zero TEC is shifted at the same point for all he receivers.
This simple application of the zero-TEC method allows a comparison of the relative sTEC measurements from the different receivers, neglecting the receiver bias components which are constant during the day and for all the satellites.
From Figure 11.15 it can be seen that the relative measurements differs, between the receivers, by up to about 10 TECU (approx. 1.6 m). One of the reason of these differences can be imputed to the different tracking architectures of the receivers, including bandwidth, correlator type, differential group delays, resulting in different satellite-specific biases as discussed in [109] and [110].

The TEC measurements from the receivers are uncalibrated and this is the reason for the large biases shown in Figure 11.14. These biases could be mostly caused by the group delay due to the receiver front end. The effect of eventual satellite residual biases should be excluded in this case or at least it should not be the primary source of bias, since the offsets show in Figure 11.14 are very different among the receivers.

This thesis wants to highlight how accurate TEC measurements are difficult to be obtained, because of the uncertainty of the calibration methods.
In the literature, in some cases the zero-TEC assumption is used as a calibration method, while in other cases a model is used, as in [111]. The Klobuchar model, for instance, sets the minimum TEC value around 10 TECU, which at times is more realistic than the zero-TEC hypothesis.
Figures from 11.16 to 11.18 show three satellites in particular, to highlight that the TEC bias between the receivers is not constant and varies also with the satellite considered. The upper plots in the Figures 11.16, 11.17 and 11.18 show the uncalibrated bias between the measurements, while the lower plots show the measurements after the application of the zero-TEC method. Notice that, for example, the CRS estimate (in the lower plot) at times goes below zero, while negative TEC measurement does not make sense physically.
In order to perform a comparison with the JPL global TEC maps, the opportune slot of the grid on the map has to be selected, corresponding to the location where the measurements were done.
The JPL map grid spacing is 2.5 degrees in latitude and 5 degrees in longitude and